Inflight Measurements in Circling Flight

Kai Rohde-Brandenburger*

German Aerospace Center (DLR), Institute of Aerodynamics and Flow Technology

Circling flight is a standard procedure during cross country flight of sailplanes. To optimize the design of sailplanes, fast and robust prediction tools are needed. To validate these tools, data of control surface deflection angles and airflow is highly desired. To gain data for validation, flight tests with the research sailplane Discus-2c DLR were conducted at different bank angles in two flights. For stabilizing the sailplane, the built-in two dimensional experimental autopilot was used. The graphs for each test section are plotted, containing rudder deflections, airflow data and inertial measurements. Averaged datapoints for each bank angle are calculated, to have validation points for steady-state calculations.

I. Nomenclature

α; AOA	=	angle of attack, deg
a_z	=	translational acceleration along z-body axis, m/s^2
A	=	wing area, m^2
β; AOS	=	angle of sideslip , deg
c_L	=	lift coefficent
c_W	=	drag coefficent
c_p	=	pressure coefficient
ω	=	angular velocity, $1/s$
ϕ, ψ, θ	=	bank, yaw, pitch angle, deg
p, q, r	=	roll-, pitch-, yaw-rate in the body coordinate system , deg/s
p_s	=	static pressure, Pa
ρ	=	air density, kg/m^3
CAS	=	calibrated airspeed, km/h
IAS	=	indicated airspeed, km/h
x, y, z	=	Position coordinates in the body coordinate system, m
V_S	=	sink rate, m/s

II. Introduction

CIRCLING flight is an important part in the design of sailplanes or other slow flying and circling aircraft. While flying cross country, up to above 50% of the time can be spend circling in thermal updrafts (Quast[8]), and even in competitions 30% of flight time (see Maughmer[4]) or 54 minutes of a three hour long flight are spent in cirling flight. The sink speed while circling is important for climbing in thermals, influencing the climb rate directly and therefore even small improvements have big effects to the overall cross country speed.
The circling polar can be derived from the straight flight polar (see Thomas[2]). This calculation is neglecting the locally varying inflow conditions due to rigid body rotion. This is causing an unevenly distritribution

*Research scientist, German Aerospace Center (DLR), Transport Aircraft, Lilienthalplatz 7, 38108 Braunschweig

of airspeed and and angle and therefore a change in Reynoldsnumber and angle of attack for each part of the plane. The deflections ot the control surfaces, needed for a steady and trimmed circling flight are also neglected. In order to improve the circling flight of modern sailplane designs, prediction tools are needed which are capable these effects in circling flight. These tools (for example Himisch[6]) are improved in the recent years, but need to be validated using flight test data from circling flight. Especially the deflection angles of the control surfaces in circling flight are influencing the lift distribution may have a big influence to the lift distribution of the wing and the horizontal and vertical fin. This influences the drag and therefore the sink rate of the sailplane, and new designs can be optimized to maximize the climb rate in thermals and therefore the cross country speed.
While the straight flight is very stable and easy to fly for long time, under circling conditions fully trimmed flight conditions at different angles of side slip can be achieved and the state of flight is not as stable as in straight flight. While flying at a defined bank angle, every rudder input is influencing every axis. The prediction tools need to trim the whole aircraft and the Center of Gravity (COG) is important for calculating the moments.
Only limited data is available in literature for modern sailplanes in circling flight or the data is simplified to the sink rate (see Merklein[5]). Measurements with the research aircraft Discus-2c DLR were conducted, to collect data of rudder angles and to measure sink rates and airflow conditions at stabilized circling flights. The data measured can be used to validate prediction tools for future sailplane designs, especially simulations of the rudder deflections under fully trimmed circling conditions.

III. Experimental Setup

The reasearch sailplane Discus-2c DLR is mainly used for flight performance measurements of other sailplanes in straight flight. Therefore the straight flight polar of the glider is well known (see idaflieg[7]). In straight flight, the glider is flown with nearly no control input. The elevator is trimmed and the glider has an inherent stability. The angle of attack (AOA) is stable at each speed and the angle of sideslip (AOS) is near to zero, only influenced by phygoid, short-period oscillations or dutch roll characteristics. In circling flight, the most values are influencing each other and make it neccesary to steer and measure all values well. Merklein[5] mentioned, that stabilized circling flights are difficult to fly for the pilot. To fly circles for longer periods at a given bank angle, it showed up that an autopilot is nessecary. The Discus-2c DLR is equipped with sensors and a data acquisition system. Also an experimental autopilot system can be used to steer two axis, commanded by a joystick on a remote control.

A. Discus-2C DLR

The Discus-2c DLR is a modern 18m class sailplane without camber changing flaps, built by the german manufacturer Schempp-Hirth. It is a modified version of the normal Discus-2c with a nose boom and an equipment bay in the fuselage, in addition to a lot smaller changes in structure. In Figure 1 the dimensions of the Discus-2c DLR are plottet and the positions of the rudder sensors are marked with a "+", and the position of the IMU and the pressure sensors are marked with a "X". The noseboom length and angle to the weighing position is given. The single seater has a wing span of 18m and a wing area of $11.39m^2$. In these test flights the weight was measured to 439.8kg and the CG was 354mm after datum point at appr. 53%.

B. Experimental Autopilot

The experimental autopilot was presented at the OSTIV-Congress[3] 2017 in detail. The actuators are mounted in the fuselage parallel to the steering rods, connected via special brackets. In Figure 2 the attachment points of the actuators are shown. It is capable of steering the elevator and ailerons up to a given force, smaller than the pilot force. The actuators are commanded by an interface control Unit (ICU), which is cappable of switching between Autopilot, direkt inputs or program sequences of rudder inputs. The ICU is translating the Inputs of the remote control to the autopilot system, which sends the commands for each rudder back to the ICU and the ICU is commanding the actuators. The autopilot system for steering and stabilising is a Pixhawk PX4 with pressure-module, connected to the pitot-static-system of the noseboom. The speed and the bank angle are commanded by the pilot via a small joystick on the remote control and then stabilized by the autopilot. The AOS is steered manually, monitored by yaw string.

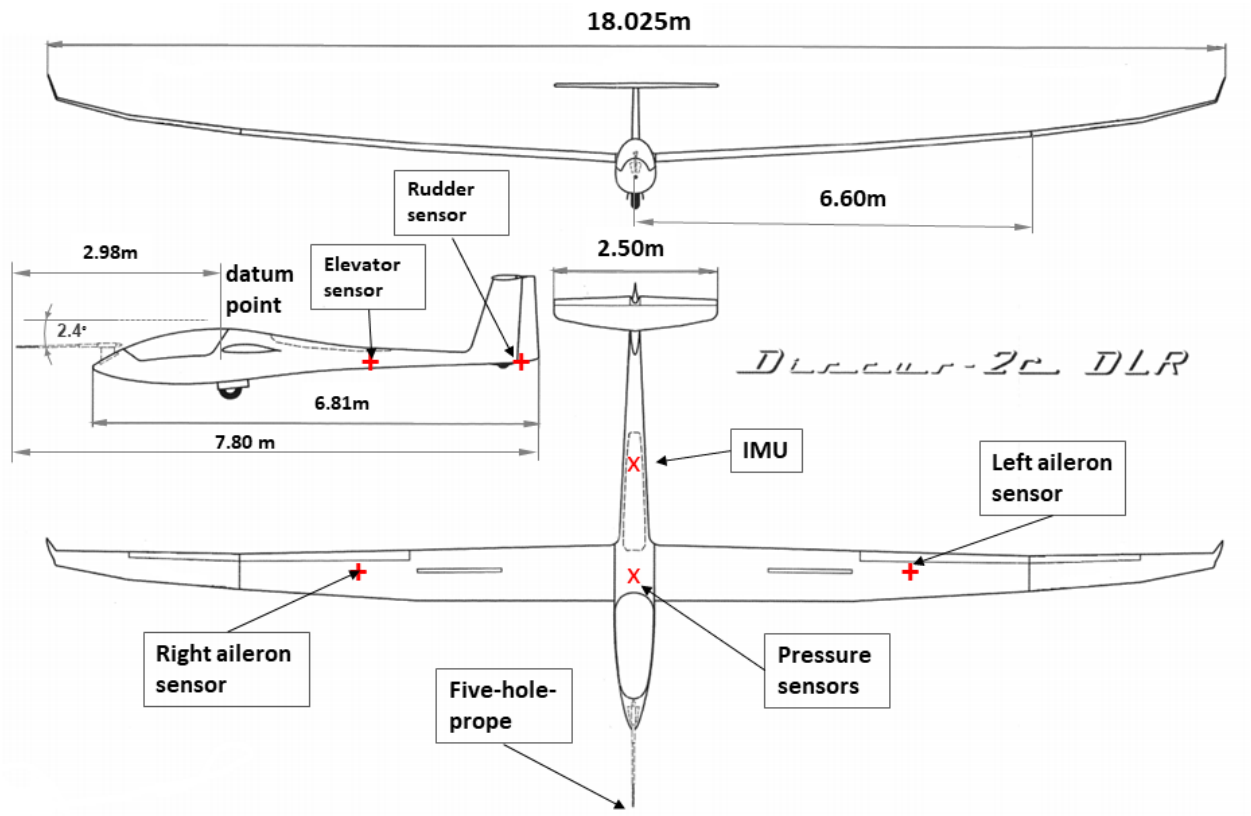

Figure 1: Discus-2c DLR: Dimensions and Rudder-Angle-Sensor Positions

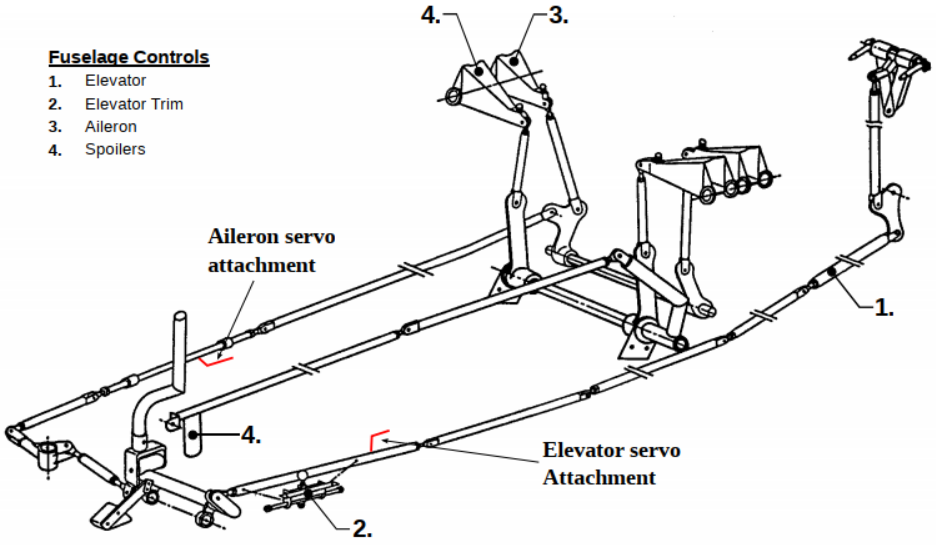

Figure 2: Attachment points of the aileron and elevator servos, edited from Maintenance Manual[9]

C. Sensors

The Discus-2c DLR is equipped with different sensors. The sensors were choosen because of accuracy, durability and space saving reasons. Most of the sensors are digital sensors, except the rudder sensors. The maximum measurement rate is therefore different. The data was downsampled to 5Hz, because faster effects of interest for this paper were not observed.

1. Pressure Sensors

The pressure sensors are mounted in the compartement behind the pilot's head. The sensors are four MENSOR CPC6100, mounted with shock absorbent rubber in horizontal orientation, to have less efects due to acceleration in z axis. The static sensor is absolute, the sensors for dynamic pressure and the alpha/beta holes at the 5-hole-probe are differential sensors. The tube length from the noseboom to the pressure transducers is about 3.2m.

2. Inertial Sensors

The inertial measurement unit (IMU) is a SBG Ellipse-E. The IMU is mounted in the back of the measurement compartement of the Discus. The transformation of coordinates is carried out internally to the center of gravity programmed. To monitor the measured values inflight, the bank angle is shown on a small display, mounted on top of the control panel.

3. Temperature/Humidity Sensor

The temperature and humidity sensor HYT939 is mounted under the right wing in a special housing to have a minimum influence of sun radiation. The housing of the sensor is speccially designed to enable the sensor to react as fast as possible to temperature and humidity changes.

4. Aileron and Elevator Sensors

To measure the angle of each aileron and the elevator, a distance measuring sensor is mounted to each rod that is directly connected to the ailerons and in the aft of the fuselage on the elevator rod. To measure the movement of the rod without adding any forces, the BAUMER OADM-12U6460 Laser distance sensor was chosen. The sensor is measuring the distance to a small carbon plate glued rectangular on the rod. The measured distance is calibrated to the angle of each rudder. This configuration allows the measurement with nearly no influence of the rod deformation due to temperature oder mechanical effects. The sensors are placed inside the wing structure without influencing the aerodynamic of the sailplane. The mechanical angle possible of the left aileron is -25 degree to +12 degree, the right aileron is -25 degree to +11degree. The maximum angle of the elevator is -22.0 degree to +15.4 degree.

5. Rudder Sensor

The rudder sensor is directly placed at the axis of the rudder. The Pewatron CP-2U is a +/-45deg contactless angle sensor with a very low torque. The sensor is calibrated to the angle of the rudder. This sensor is placed inside the tail without influencing the aerodynamic of the sailplane too. The maximum mechanically possible angles of the rudder are +30.0 degree to the right and -30.6 degree to the left.

IV. Methodology

The measurements for one bank direction (left or right) were done in a row. Before and after the circling test sections to one direction, a straight flight with zero degree bank angle was performed to compensate the measurement for air mass movements and calibration of the sensors.
The plane was weighted with the pilot on July 23rd 2019 and trimmed to the center of gravity wanted. The measurements were conducted on two days, July 24th and 25th 2019 on the Braunschweig research airport (ICAO-Code: EDVE) The test flight started in calm morning airmasses and the glider was towed to FL95. The measurement time for each test section was between 90 to 130 seconds. The speed for each test point was calculated beforehand, to have all measurements near to C_L=0.85. This resulted in prescribed indicated airspeeds for each bank angle, varying from 95-118km/h CAS (see table 3 and 4).

A. Straight Flight

To be able to observe errors and eventually calibrate the measurements, the tests in straight flight offer the option to check the values at zero bank angle. Also the influence of air mass movenments can be observed, because the sinkspeed of the Discus-2c DLR is known in straight flight (idaflieg[7]).

The straight flight test sections were stabilized and flown for 90 seconds manually without the autopilot. After a stabilized straight flight with autopilot, the test points with positive or negative bank angle were flown. Table 2 shows the desired flight conditions and the measured values of the straight sections of both flights, averaged over the duration of each test section.

Table 2. Overview of straight flight test sections of flight #1 and #2

testpoint #	target bank angle degree	target CAS km/h	target duration seconds	meas. bank angle degree	meas. CAS km/h	meas. C_L -	meas. duration seconds
1.1	0	95.0	60	0.1	97.4	0.84	77
1.8	0	95.0	60	1.0	96.9	0.85	65
1.15	0	95.0	60	-0.4	101.3	0.78	30
2.1	0	95.0	60	-0.8	98.2	0.83	45
2.12	0	95.0	60	-0.4	97.2	0.85	89

B. Circling Flight

The measurements in circling flight were planned to be in steps of 5 degrees to the right (positive values) and to the left (negative values). The steps were flown in 10 degrees, because each stabilization of a bank angle took to much time due to the corresponding speed change neccesary and the time for adjusting the autopilot. The test points were stabilized by the autopilot, with the exception of the AOS, which was stabilized by the pilot. Table 3 and Table 4 show the desired flight conditions and the measured values of the circling sections of both flights, averaged over the duration of each test section.

Table 3. Overview of averaged circling flight test sections of flight # 1

testpoint #	target bank angle degree	target CAS km/h	target duration seconds	meas. bank angle degree	meas. CAS km/h	meas. C_L -	meas. duration seconds
1.2	10	96.0	90	11.5	99.0	0.84	120
1.3	20	98.0	90	19.4	104.2	0.79	93
1.4	30	102.0	90	32.0	97.4	0.73	53
1.5	40	108.0	90	39.9	112.9	0.80	68
1.6	45	113.0	90	41.7	118.6	0.75	56
1.7	50	118.0	90	50.3	123.9	0.81	78
1.9	-10	96.0	90	-12.9	96.8	0.88	69
1.10	-20	98.0	90	-23.8	100.6	0.86	47
1.11	-30	102.0	90	-33.7	107.71	0.83	73
1.12	-40	108.0	90	-36.1	110.0	0.82	52
1.13	-45	113.0	90	-45.1	125.2	0.72	38
1.14	-50	118.0	90	-54.2	129.9	0.81	74

The desired endurance of each test point is varying, depending on the stabilized time without any big deviations in speed, rudder inputs or bank angle. Each testsection was evaluated and the best stabilized part was taken for evaluation. In some testsections, the sailplane was stabilized by the autopilot well, and the section was flown for a much longer time than prescribed.

V. Data Preparation

The Discus-2c DLR is calibrated for straight flight. The CAS in the measurement is taken from the calibrated noseboom, but the pilot stabilizes the plane at IAS readings from the standard pitot-static-

Table 4. Overview of averaged circling flight test sections of flight # 2

testpoint #	target bank angle degree	target CAS km/h	target duration seconds	meas. bank angle degree	meas. CAS km/h	meas. C_L -	meas. duration seconds
2.2	10	96.0	90	12.9	98.37	0.85	100.8
2.3	20	98.0	90	19.2	102.34	0.81	77
2.4	30	102.0	90	28.3	107.55	0.80	60
2.5	40	108.0	90	38.0	111.5	0.81	199
2.6	50	118.0	90	48.8	118.6	0.87	113
2.7	-10	96.0	90	-11.4	98.6	0.84	121
2.8	-20	98.0	90	-23.5	102.8	0.82	89
2.9	-30	102.0	90	-31.4	102.1	0.89	73
2.10	-40	108.0	90	-44.4	115.3	0.84	70
2.11	-50	118.0	90	-49.4	120.46	0.84	98

system, which can lead to differences in indicated and measured airspeeds. At circling flight conditions, the noseboom and the center of gravity of the plane is circling around the middle of the circle. Each part of the plane, not in the center of gravity is moving because of the distance to the cg-point and the rotation of the plane. This induces speeds and angles in the measurements , and the data has to be corrected by geometrical calculations with data from the IMU. The correction is already calculated in the values averaged and in the graphs, marked with "corrected".

A. Pressure Data

The data from the pressure sensors is used for CAS, static pressure and the angles, calculated from the diffential pressure readings from the 5-hole-Probe. The offset of the sensors is evaluated shortly before the takeoff, when the sensors warmed up at least 15 minutes and the noseboom was covered due to wind errors.

B. AOA and AOS Correction

The angles are calculated from pressure measurements at the noseboom and are influenced by the additional speeds in circling flight. The angles can be corrected with the measurements from the IMU-gyroscopes and are recalculated to the center of gravity via formulas (1)-(6). The additional speed at the nose boom can be calculated by the turning speed indication of the IMU and the distance of the nose boom to the center of gravity via formula (7). In this case, the distance of the Five-Hole-head to the datum point is 2980mm, and the distance of the CG to datum point is 354mm. The calculation has to be corrected for density influences. For each axis the additional movement of the top of the noseboom has to be calculated.
It should be mentioned, that the measured AOA of the noseboom is influenced by the induced flow field of the sailplane, especially by the wing, due to the lift generating surfacec. These values have to be corrected, if used for validation. This has not been corrected in this paper.

$$V_{z,q} = q\frac{2\pi(l_{noseboom} + l_{CG})}{360^\circ}\sqrt{\frac{\rho_{act}}{\rho_{MSL}}} \tag{1}$$

$$V_{y,r} = r\frac{2\pi(l_{noseboom} + l_{CG})}{360^\circ}\sqrt{\frac{\rho_{act}}{\rho_{MSL}}} \tag{2}$$

The additional angles at the noseboom due to yaw and pitch rates, measured by the IMU, can be calculated with equation (3) and equation (4):

$$\alpha_q = \sin\frac{V_{z,q}}{V_{CAS}} \tag{3}$$

$$\beta_r = \sin\frac{V_{y,r}}{V_{CAS}} \tag{4}$$

The AOA and AOS in the center of gravity can be calculated with equation (5) and equation (6) while in (5) the mounting angle of the noseboom is added:

$$\alpha_{CG} = \alpha_{measured} + \alpha_q - 2.4^\circ \tag{5}$$

$$\beta_{CG} = \beta_{measured} + \beta_r \tag{6}$$

The corrected airspeed can be calculated with equation (7) :

$$V_{CAS_{corrected}} = \sqrt{V_{CAS}^2 - V_{y,\dot{\psi}}^2 - V_{z,\dot{\psi}}^2} \tag{7}$$

C. Rudder Angles

The rudder values are measured by analog sensors near each rudder. The rudder angles were calibrated direct after the second flight and the corrected values are used. The machanical coupling between each aileron can differ over the flight, because of wingbending, g-loads and temperature influences to the connection rods. Therefore each aileron has its own sensor, very near to the connection of the rod. The rudder sensor is directly connected to the rudder-axis. The elevator sensor is in the rear fuselage at the connection rod around 2.5m before the direct connection to the elevator.

VI. Measured Data

The data was recorded over the whole flight time. Afterwards, each test section was analysed and only the stabilized periods were used for evaluation. The data of each section is plotted in graphs and added in the Appendix. Due to the amount of data, only a few measurement sections are discussed. The data and graphs of all measurement sections are in the Appendix. Also the calculated standard deviations, environmental data and accelerations can be found in Table 8 and Table 9.

A. Straight Flight

In calm air and stabilized straight flight the measurement data shows the influence of the airmass to the sensors and even in straight flight, the resolution of the sensors is capable to detect movements. Even small turbulences cause inputs to stabilize the speed and the bank angle. From pilot view, the straight flight feels very stable and calm, but in the measurement data the small inputs and the bank angle deviations can be shown. In Figure 3, in straight flight the bank angle varied between -1 degree to +1 degree over 77 seconds, while the CAS is influenced by slight turbulence at the beginning and varied between 96 km/h and 98 km/h. The influence of the slight turbulence can also be observed in the AOA and AOS readings.

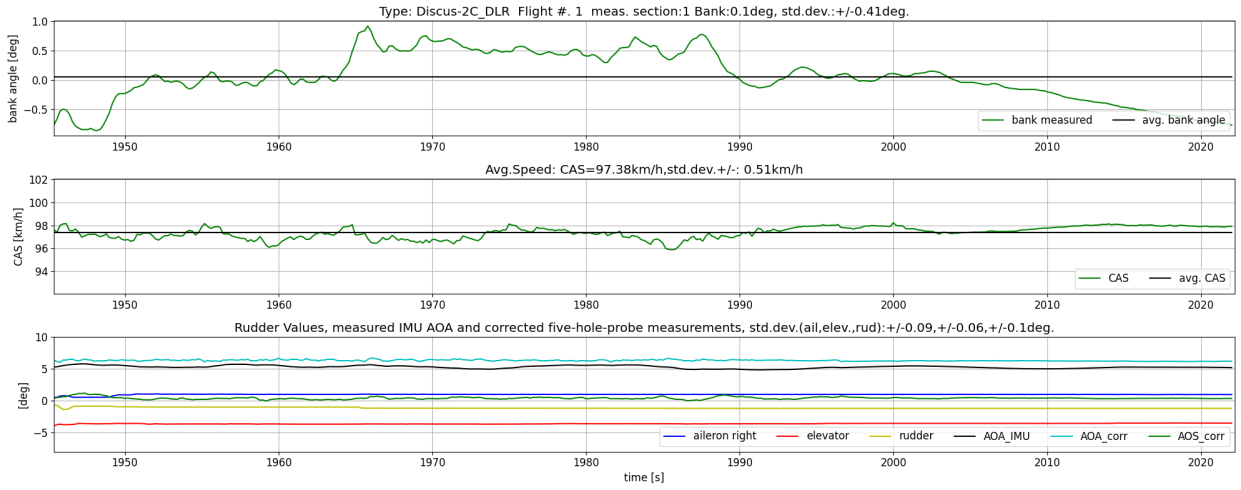

Figure 3: Section 1.1; overview of measured values

In Figure 4 the bank angle varied between +3 degree and -1 degree, the CAS is between 95 km/h and 98 km/h, while the rudder movements are slightly bigger than in section 1.1 in Figure 3.

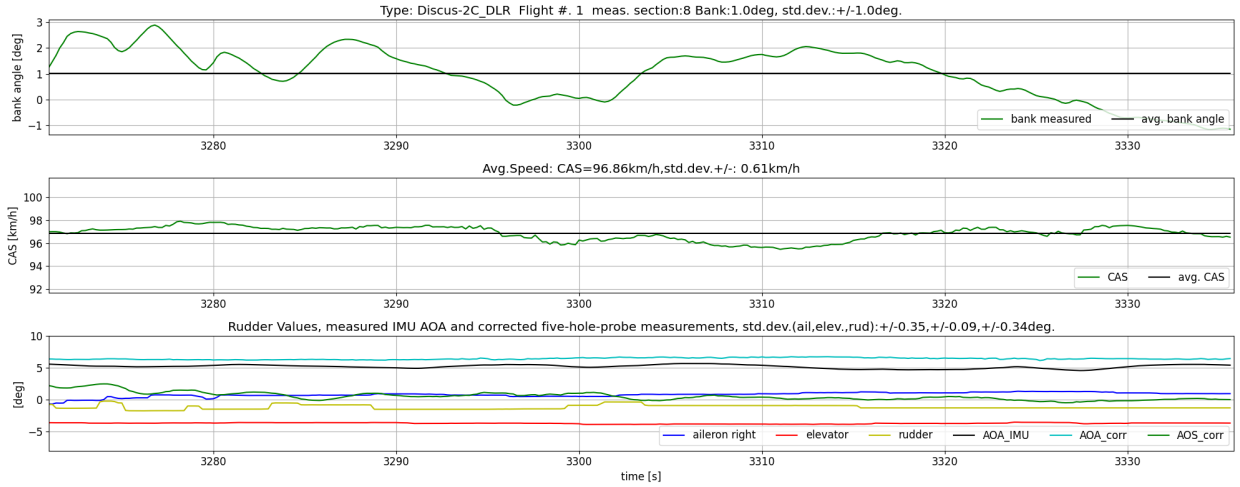

Figure 4: Section 1.8; overview of measured values

B. Circling Flight

The most measurements are stabilized well and the inputs of the autopilot system can be observed in the graphs. The pilot holds the yaw-string centered, resulting in slightly different AOS for each test section. It took time to stabilize the different speeds for each test point and resulted in a loss of height between each test section due to stabilizing time. In Table 8 and Table 9 the averaged altitude of each measurement section can give an overview over the altutude needed.

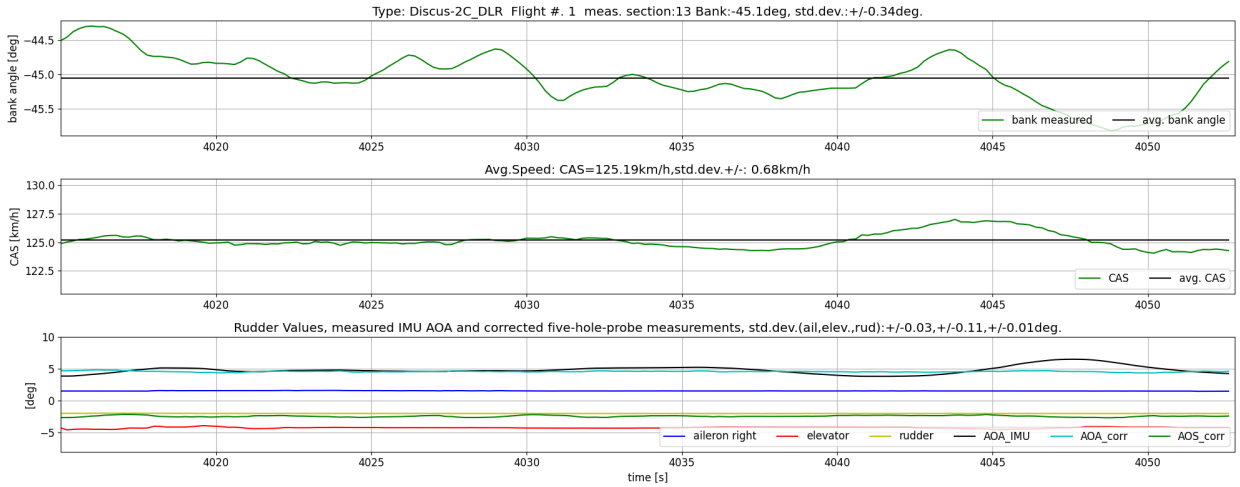

Figure 5: Section 1.13; overview of measured values

In Figure 5 the bank angle varied from -44.3 degree to -45.9 degree over a time of 38 seconds and the CAS varied between 124km/h and 127km/h. Only inputs to the elevator can be observed. In Figure 6 the bank angle varied between -29.5 degree and -34 degree, while the CAS varied between 99km/h and 104km/h over 73seconds. The input of the autopilot can be observed in the aileron deflections.

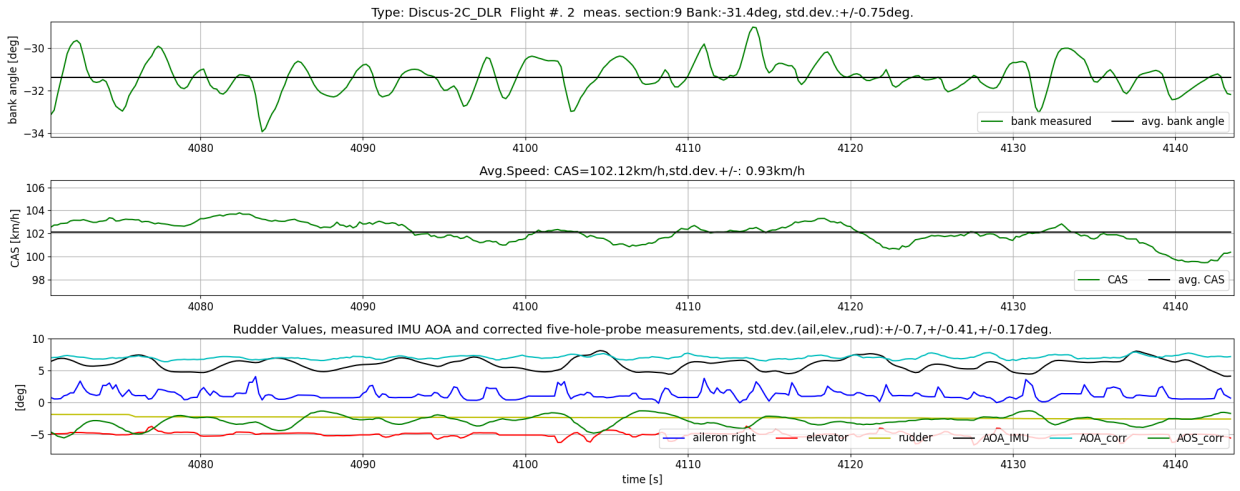

Figure 6: Section 2.9; overview of measured values

C. Sink Rates

The sink rate can be read from the measured straight flight polar from idaflieg.[7] The sinkspeed measured has to be corrected for weight and density influences according to Thomas.[2] The difference between the sink rates at zero bank angle from the polare and the measured sink rate from pressure readings can be assumed to be the metheorological air mass sink rate. But it should be mentioned, that this can only give an overview over the errors in the measured sinkrates due to changes in air mass sink rates in every test section. Therefore, this correction was not included and only the measured values are plotted.

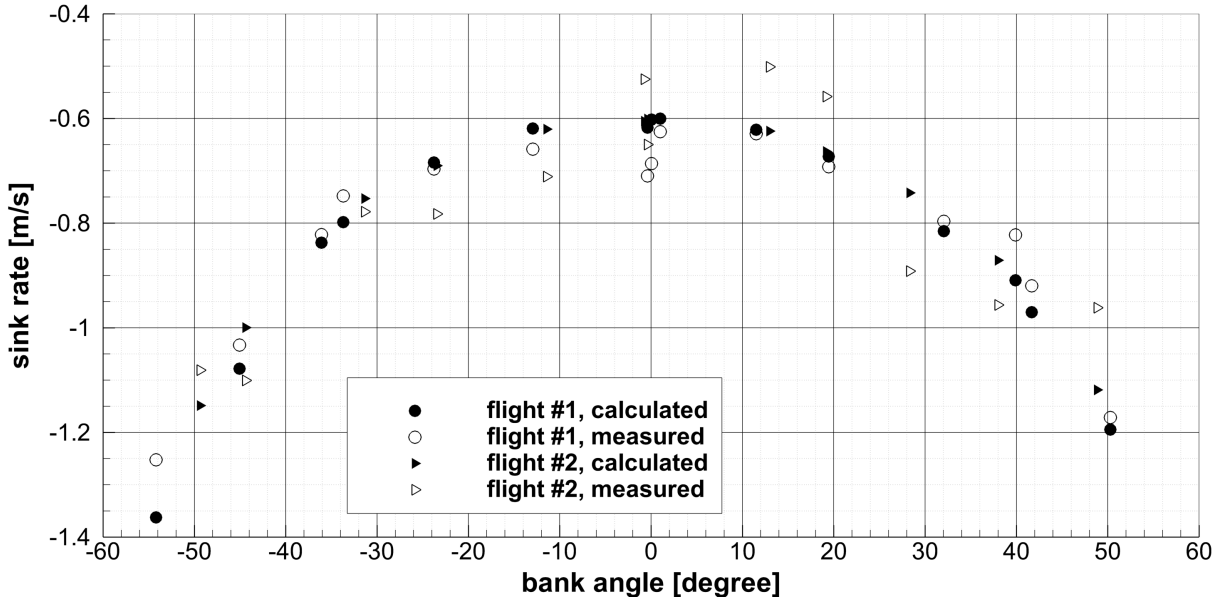

Figure 7: Measured and calculated sinkrates for circling flights of the Discus-2c DLR

The sink rate, calculated from the straight flight polar uses only the measured bank angle. The sink rate from pressure measurement is only averaged over the section length, and therefore the section time should be considered in Figure 7. In this figure the sinkrate, derived from the straight flight polar and the measured sinkrate for each test section is plotted over the bank angle. A bigger variation in flight number 2 can be observed, while flight number 1 seems very smooth. Merklein[5] metioned, that there is no big influence

between the measured data of a K8 and the calculated values, but most of the measured points with the Discus-2c DLR have a smaller sinkrate than the calculated values from the straight flight polar. To have a more detailed view on this, the differences are plotted in Figure 8. A positive value means less sinkrate than the sink rate derived from the straight flight polar. The weather error at zero bank angle can be observed and may cause the variation of the values to the quadratic compensation curve. Even in flight number 2, at high bank angles, a sink rate smaller than the sink rate calculated from the straight flight polar can be observed. Due to the very small aileron deflections, it may show the reynoldsnumber effect at higher speeds, neglected in the calculated values from the straight flight polar.

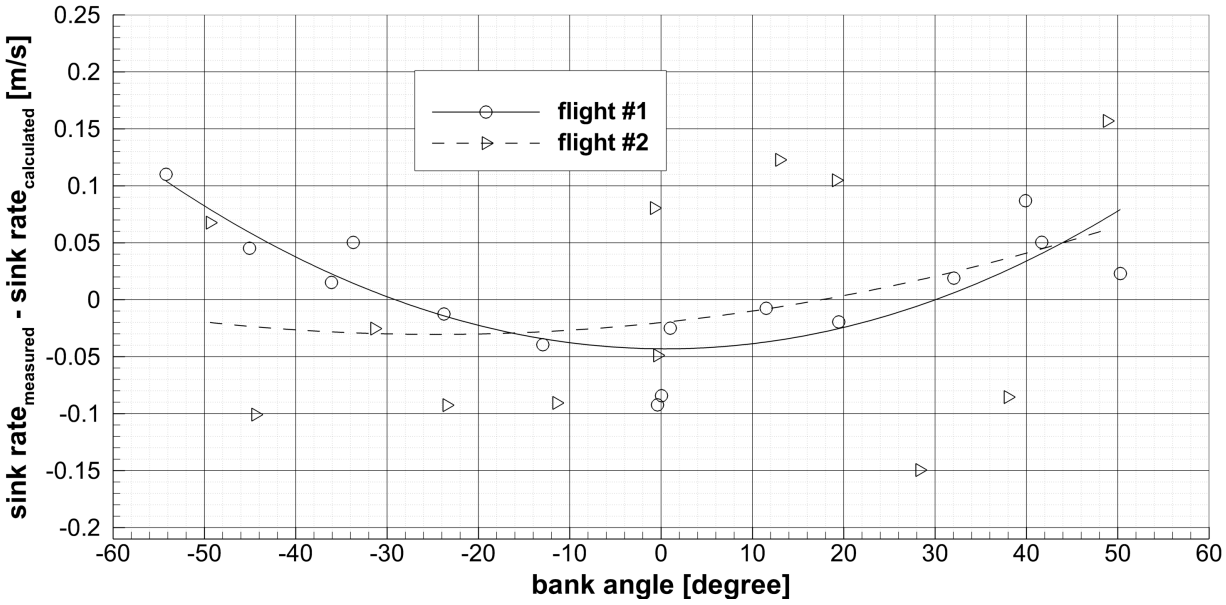

Figure 8: Differences in measured and calculated sinkrates for circling flights of the Discus-2c DLR

VII. Conclusion

Measurements in circling flight could be succesfull conducted with the Discus-2c DLR. The measurements show small variations in rudder deflections and airflow. Values for 27 different bank angles from -54.2 degree to +50.3 degree could be measured. Averaged values for each test section are calculated and detailed measurement data for each section is shown.

The calculated sink rates for banked flight from the measured straight flight polar and the measured sink rates at bank angle are plotted. The differences between the calculated and the measured sink rates in flight number 1 show less drag and therefore less sinkrate for the Discus-2c DLR in circling flight than calculated from the straight flight polar. This may come from Reynoldsnumber effects, which is neglected in the calculation.

Because sailplanes spend in most cases over 30% of flightime in circling flight, even small changes in sinkrate can make a big influence to the cross country speed possible. Optimizations of sailplane designs for circling flight are only possible with simulation programs which can take these effects into account. The measured values in this paper can be used to validate these programs.

References

[1]B. Müller *Design study of a sailplane with fowler flaps.* (German) [*Entwurfsstudie für ein Segelflugzeug mit Flächenklappen*]. DFVLR, Inst. f. Aerodynamik, Studienarbeit, 1982.

[2]F. Thomas *Fundamentals of Sailplane Design.* (German) [*Grundlagen für den Entwurf von Segelflugzeugen*]. Motorbuch Verlag Stuttgart, 2. Auflage, 1985.

[3]K. Rohde-Brandenburger *Actuators in the Discus-2c DLR: Experimental autopilot for research.* Lecture at the OSTIV-Congress, Benalla, Australia, 2017

[4]M. Maughmer, J. Coder, C. Wannenmacher, W. Würz *The Design of a New Racing Saiplane: A New Thermal Mix Model*

and the Role of Transitional CFD. AIAA AVIATION Forum, Denver, Colorado, 2017

[5]H. J. Merklein *Comparison of Circling Flight Performance of Sailplanes with measured straight flight polars.*(German) [*Vergleich der Kreisflugmessungen einiger Segelflugzeuge aufgrund vermessener Flugpolaren*]. Technischer Vermerk S 2/65, Lecture at the OSTIV-Congress, South Cerny, England, June 1965

[6]J. Himisch, K. Rohde-Brandenburger *Circling Calculations for Predesign of Sailplanes*. Lecture at the OSTIV-Congress, Hosin, Czech Republic, 2018

[7]idaflieg, DLR *Flight performance measurement of the Discus-2c DLR, D-9833.*(German) [*Flugleistungsvermessung Discus-2c DLR, D-9833, nach dem Vergleichsflugverfahren*]. idaflieg, Stendal, August 2015

[8]A. Quast *Cross-Country-Speed of measured sailplanes with four new thermal updraft models taken into account.*(German) [*Mittlere Reisegeschwindigkeit vermessener Segelflugzeuge unter gleichzeitiger Berücksichtigung von vier Modellaufwindverteilungen*]. Akademische Fliegergruppe Braunschweig, Oktober 1977

[9]Schempp-Hirth Flugzeugbau *preliminary Maintenance manual for the Discus-2c DLR* .(German) [*vorläufiges Wartungshandbuch für das Segelflugzeug Discus-2c DLR*]. Schempp-Hirth Flugzeugbau GmbH, Januar 2005

Acknowledgments

The author would like to thank Dr. Erik Braun and the German Aerospace Flight experiments facility for the supports and towing in the flight tests. Also the students of the Academic Flying Group (Akaflieg) Braunschweig supported the flight tests in their spare time.

Appendix

A. Averaged values of straight flight sections of Flight #1 and #2:

Table 5. Averaged values of straight flight sections

Nr.	meas.	meas.	meas.	meas.	meas..	meas..	meas..	meas.	polar	calc	meas.
#	bank	CAS	α_{corr}	β_{corr}	ail.right	ail.left	rud.	elev.	$V_{S,polar}$	$V_{S,calc}$	$V_{S.Baro}$
-	deg.	km/h	deg.	deg.	deg.	deg.	deg.	deg.	m/s	m/s	m/s
1.1	0.05	97.38	6.30	0.40	0.96	-1.24	-1.14	-3.61	0.602	0.602	0.845
1.8	1.00	96.86	6.42	0.53	0.80	-1.35	-1.17	-3.70	0.600	0.600	0.625
1.15	-0.40	101.27	5.49	-0.74	1.39	-1.85	-0.78	-2.96	0.617	0.617	0.710
2.1	-0.76	98.23	6.06	0.40	1.01	-1.14	-1.20	-3.36	-0.605	-0.605	-0.525
2.12	-0.40	97.22	6.45	-1.33	1.81	-2.11	-0.69	-3.39	-0.602	-0.601	-0.650

B. Averaged values of circling flight sections of Flight #1 and #2:

Table 6. Averaged values of circling flight sections of flight #1

Nr.	meas.	meas.	meas.	meas.	meas..	meas..	meas..	meas.	polar	calc	meas.
#	bank	CAS	α_{corr}	β_{corr}	ail.right	ail.left	rud.	elev.	$V_{S,polar}$	$V_{S,calc}$	$V_{S.Baro}$
-	deg.	km/h	deg.	deg.	deg.	deg.	deg.	deg.	m/s	m/s	m/s
1.2	11.50	98.98	6.61	-3.41	3.06	-3.89	0.90	-3.55	0.608	0.622	0.629
1.3	19.44	104.22	5.70	-2.38	2.67	-3.47	1.20	-3.33	0.632	0.673	0.692
1.4	32.04	113.49	4.79	2.58	0.30	-0.72	-0.47	-3.49	0.692	0.815	0.796
1.5	39,89	112.92	5.77	2.85	0.55	-0.95	-0.03	-4.74	0.688	0.909	0.822
1.6	41.68	118.57	5.16	1.95	0.83	-1.25	0.19	-4.35	0.737	0.970	0.920
1.7	50.28	123.93	5.61	1.27	1.27	-1.66	0.72	-5.43	0.786	1.195	1.171
1.9	-12.95	96.80	6.73	1.31	-0.24	-0.19	-2.37	-4.26	0.600	0.619	0.659
1.10	-23.78	100.58	6.62	-1.71	0.84	-1.35	-1.95	-4.44	0.614	0.684	0.696
1.11	-33.70	107.71	6.08	-1.95	0.96	-1.41	-2.26	-4.70	0.652	0.798	0.748
1.12	-36.09	110.04	5.86	-1.58	0.81	-1.19	-2.41	-4.68	0.667	0.837	0.822
1.13	-45.05	125.19	4.56	-2.44	1.53	-1.93	-2.01	-4.25	0.799	1.078	1.033
1.14	-54.20	129.87	5.40	-1.23	0.96	-1.02	-2.76	-5.88	0.851	1.362	1.252

Table 7. Averaged values of circling flight sections of flight #2

Nr.	meas.	meas.	meas.	meas.	meas..	meas..	meas..	meas.	polar	calc	meas.
#	bank	CAS	α_{corr}	β_{corr}	ail.right	ail.left	rud.	elev.	$V_{S,polar}$	$V_{S,calc}$	$V_{S.Baro}$
-	deg.	km/h	deg.	deg.	deg.	deg.	deg.	deg.	m/s	m/s	m/s
2.2	12.95	98.37	6.63	-2.73	2.90	-3.49	0.64	-3.62	0.606	0.624	0.501
2.3	19.17	102.34	6.03	-2.31	2.76	-3.41	0.73	-3.48	0.622	0.663	0.558
2.4	28.30	107.55	5.86	-2.78	3.01	-3.76	1.45	-3.72	0.652	0.742	0.892
2.5	37.97	111.50	5.86	1.93	1.05	-1.42	0.04	-4.60	0.678	0.871	0.956
2.6	48.82	118.63	6.32	-0.70	2.33	-2.76	1.35	-5.79	0.735	1.119	0.962
2.7	-11.45	98.59	6.28	2.38	-0.68	0.38	-2.72	-3.70	0.607	0.621	0.711
2.8	-23.47	102.83	6.14	-2.07	1.31	-1.73	-2.02	-3.86	0.625	0.690	0.783
2.9	-31.38	102.12	7.05	-2.88	1.21	-1.56	-2.36	-5.03	0.621	0.753	0.778
2.10	-44.41	115.33	6.07	-2.46	1.19	-1.40	-2.53	-5.29	0.706	1.000	1.100
2.11	-49.38	120.46	5.96	-2.36	1.30	-1.41	-2.74	-5.69	0.751	1.149	1.081

C. Environmental and Atmospheric data and standard deviations of Flight #1 and #2:

Table 8. Data and Standard Deviations of measured values of flight #1

Nr. # -	dev. bank ±deg.	dev. CAS ±km/h	dev.. ail.right ±deg.	dev.. ail.left ±deg.	dev. rud. ±deg.	dev. elev. ±deg.	meas. temp. deg.C.	meas. density kg/m^3	meas. accel. m/s^2	meas. GPS alt. m
1.1	0.41	0.51	0.09	0.09	0.10	0.06	11.21	0.881	9.81	2787.5
1.2	1.29	2.34	0.39	0.47	0.33	0.49	12.81	0.916	10.08	2435.7
1.3	0.62	1.23	0.57	0.70	0.92	0.41	13.73	0.933	10.45	2260.4
1.4	0.72	0.56	0.58	0.66	0.02	0.46	14.22	0.945	11.45	2143.1
1.5	0.94	0.98	0.68	0.78	0.02	0.43	14.81	0.954	12.56	2047.3
1.6	0.85	5.36	0.57	0.65	0.14	0.67	15.42	0.966	12.96	1931.9
1.7	1.73	3.47	0.78	0.88	0.60	0.71	15.85	0.984	15.19	1756.7
1.8	1.00	0.61	0.35	0.39	0.34	0.09	15.60	1.003	9.82	1599.1
1.9	0.51	0.71	0.02	0.02	0.01	0.09	16.59	1.017	10.11	1458.8
1.10	0.76	1.30	0.29	0.36	0.01	0.20	17.38	1.025	10.69	1374.5
1.11	1.70	1.18	0.07	0.07	0.05	0.22	18.43	1.036	11.75	1255.3
1.12	0.76	1.01	0.07	0.10	0.15	0.12	19.67	1.048	12.10	1130.5
1.13	0.34	0.68	0.03	0.03	0.01	0.11	21.07	1.064	13.75	960.7
1.14	0.93	1.68	0.25	0.34	0.18	0.19	22.22	1.076	16.73	836.8
1.15	0.62	0.80	0.35	0.45	0.47	0.08	22.22	1.076	9.81	740.2

Appendix

Table 9. Data and Standard Deviations of measured values of Flight #2

Nr. # -	dev. bank ±deg.	dev. CAS ±km/h	dev.. ail.right ±deg.	dev.. ail.left ±deg.	dev. rud. ±deg.	dev. elev. ±deg.	meas. temp. deg.C.	meas. density kg/m^3	meas. accel. m/s^2	meas. GPS alt. m
2.1	0.46	0.60	0.12	0.15	0.04	0.03	12.07	0.875	9.80	2820.4
2.2	0.47	1.23	0.34	0.43	0.92	0.14	14.11	0.896	10.10	2579.5
2.3	0.63	0.40	0.53	0.67	0.08	0.00	14.90	0.906	10.44	2472.4
2.4	1.02	3.13	0.59	0.76	0.35	0.51	16.58	0.928	11.28	2235.0
2.5	1.72	3.95	1.00	1.14	0.62	0.71	17.93	0.947	12.33	2029.7
2.6	1.52	2.56	0.80	0.93	0.21	0.61	18.24	0.970	14.97	1812.3
2.7	0.67	3.07	0.90	0.92	0.31	0.58	18.61	0.996	10.05	1570.6
2.8	0.80	1.22	0.57	0.67	0.17	0.36	19.48	1.012	10.67	1417.6
2.9	0.75	0.93	0.70	0.82	0.17	0.41	20.81	1.024	11.41	1280.2
2.10	0.65	1.02	0.47	0.55	0.01	0.40	22.43	1.041	13.62	1099.0
2.11	0.70	1.31	0.47	0.55	0.16	0.34	24.09	1.057	14.89	928.5
2.12	0.73	0.84	0.34	0.43	0.42	0.11	25.53	1.068	9.83	802.8

D. Measurement data plots of all measurment sections of Flight #1:

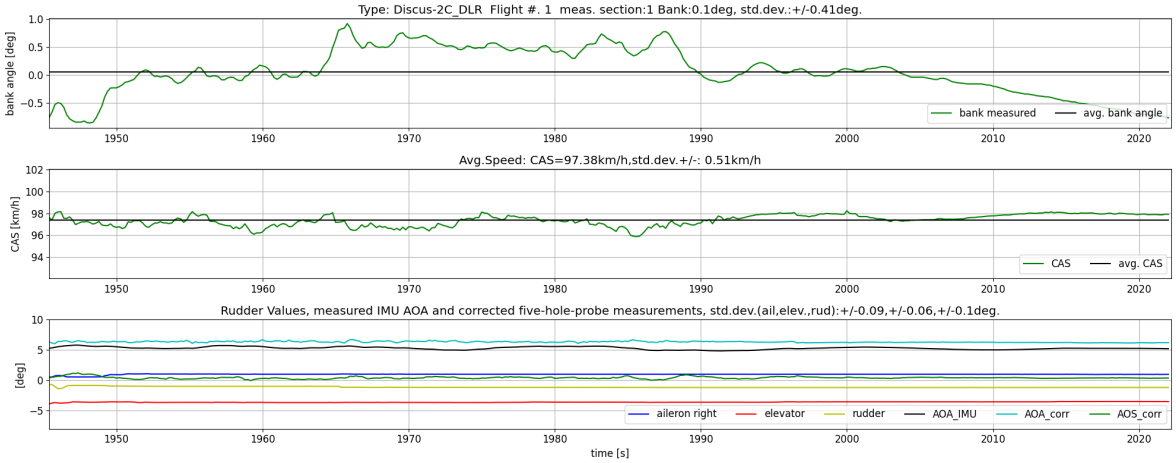

Figure 9: Section 1.1; overview of measured values

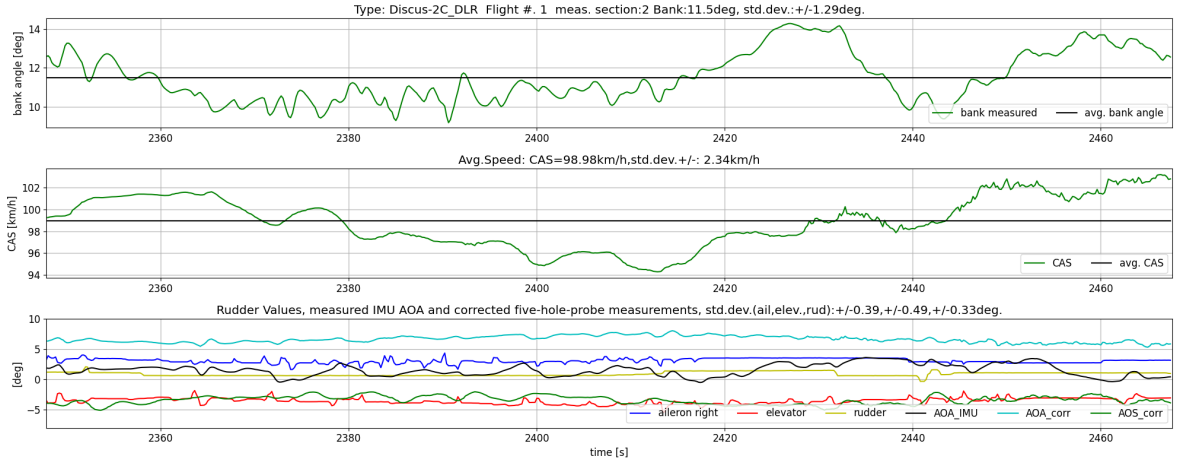

Figure 10: Section 1.2; overview of measured values

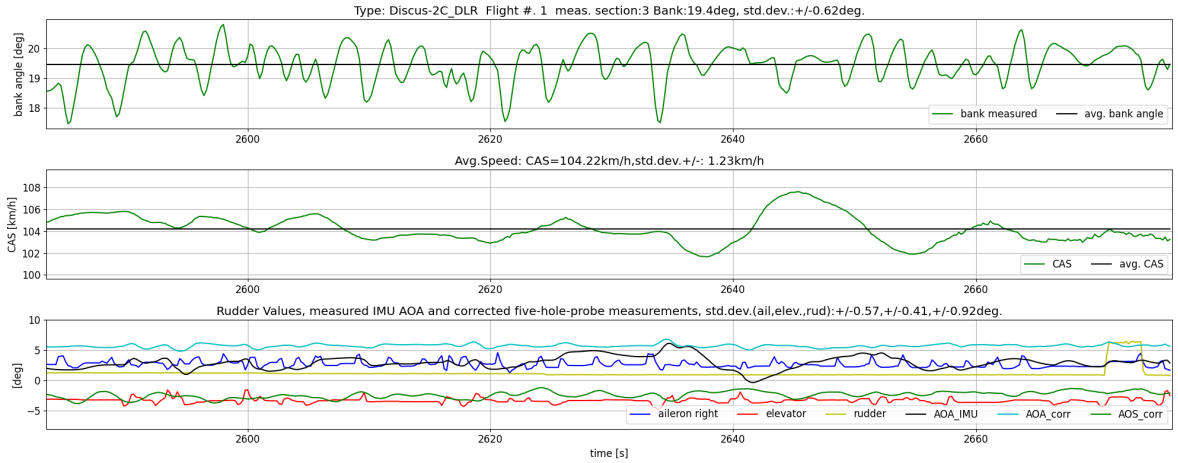

Figure 11: Section 1.3; overview of measured values

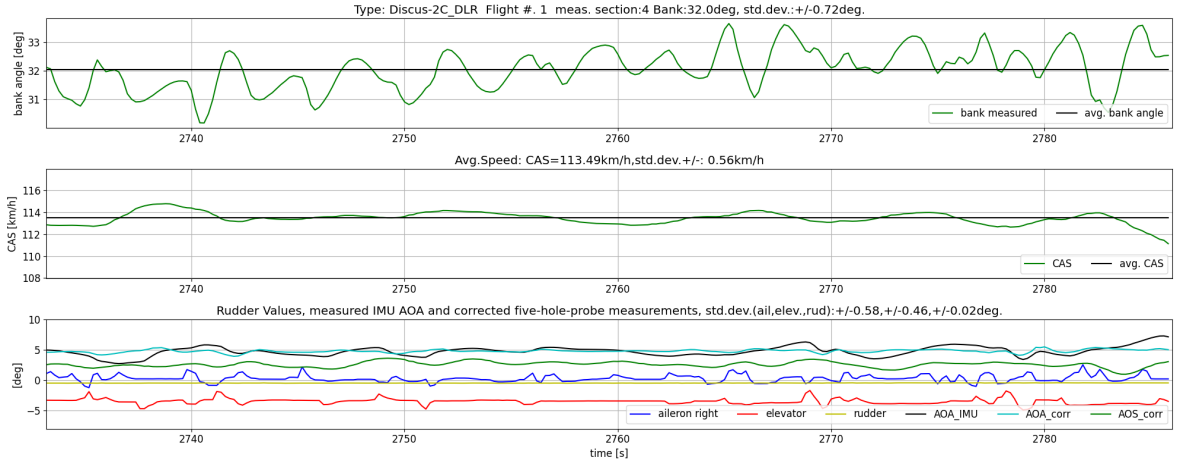

Figure 12: Section 1.4; overview of measured values

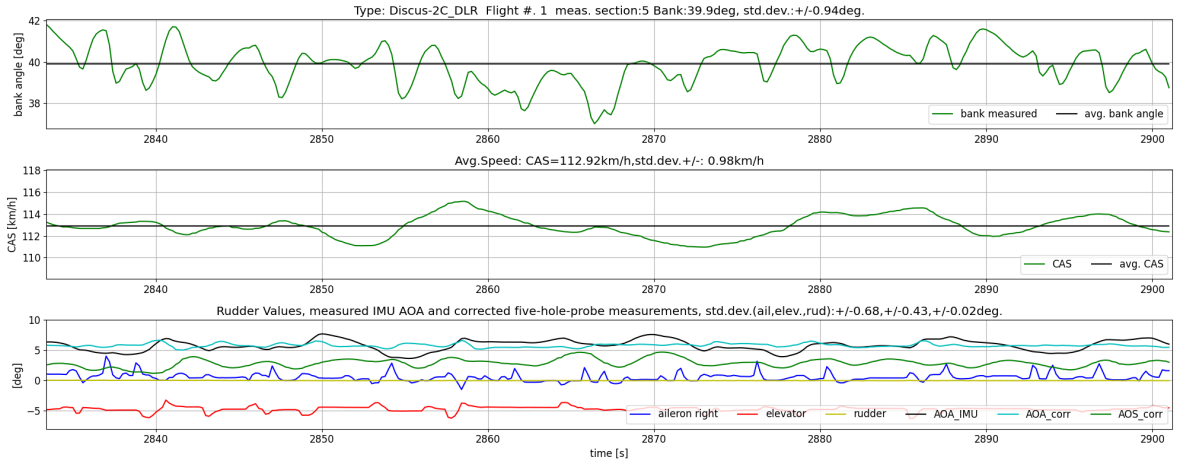

Figure 13: Section 1.5; overview of measured values

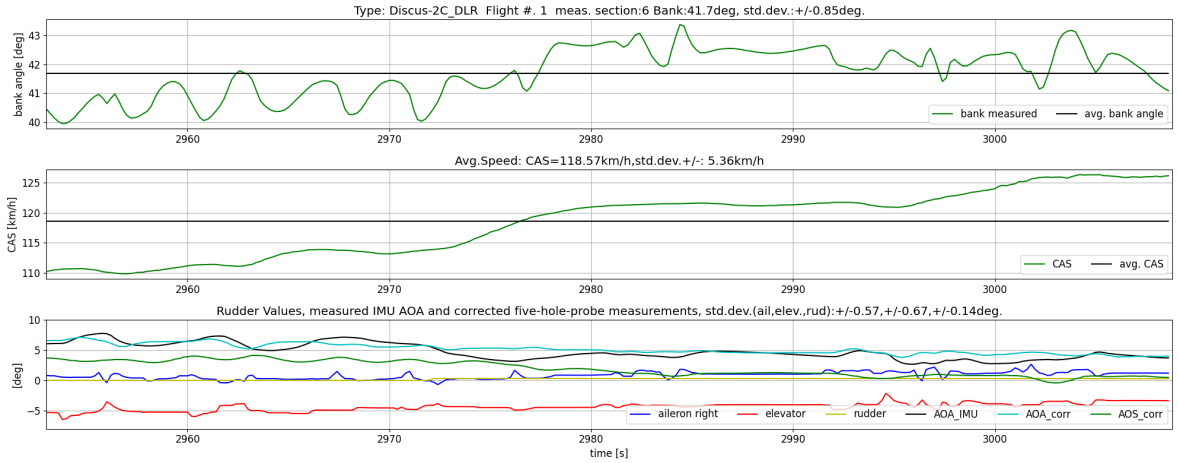

Figure 14: Section 1.6; overview of measured values

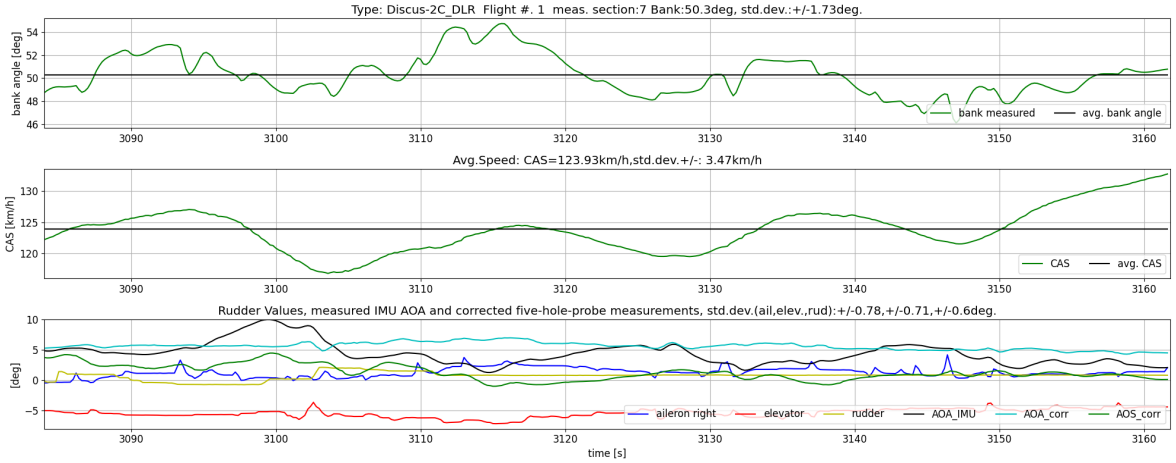

Figure 15: Section 1.7; overview of measured values

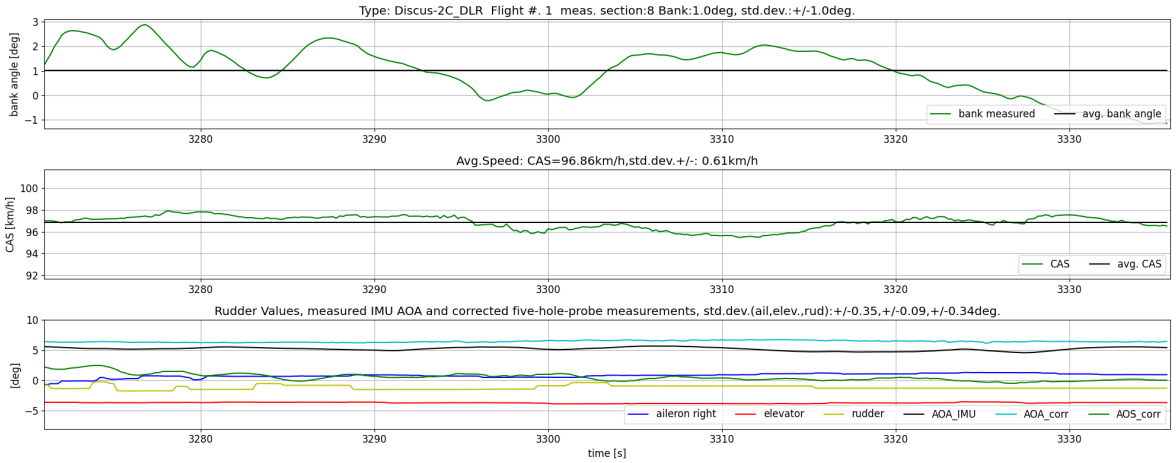

Figure 16: Section 1.8; overview of measured values

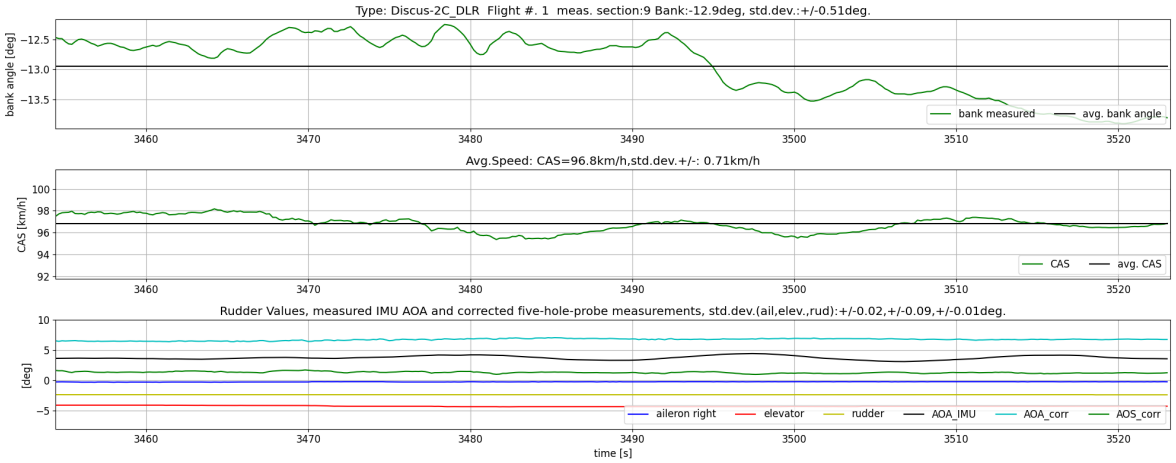

Figure 17: Section 1.9; overview of measured values

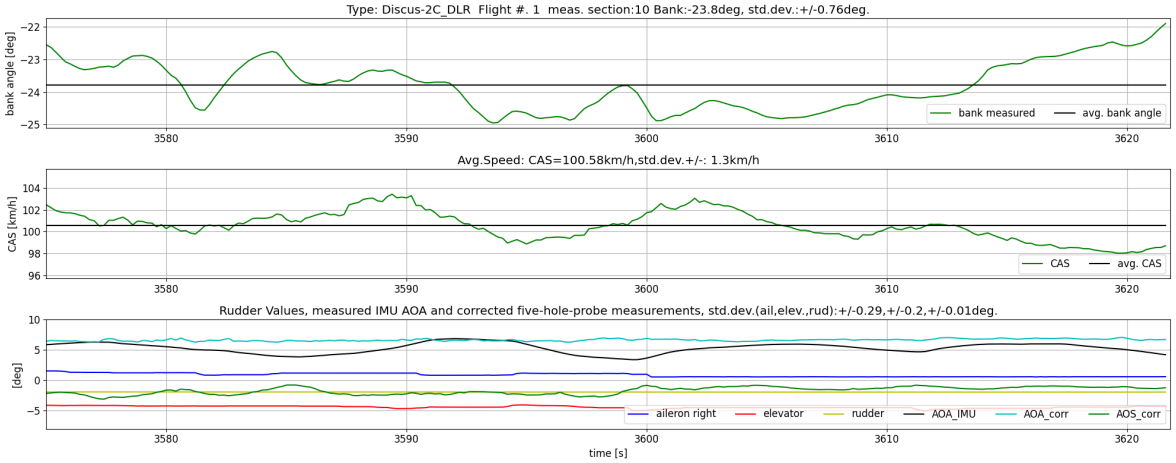

Figure 18: Section 1.10; overview of measured values

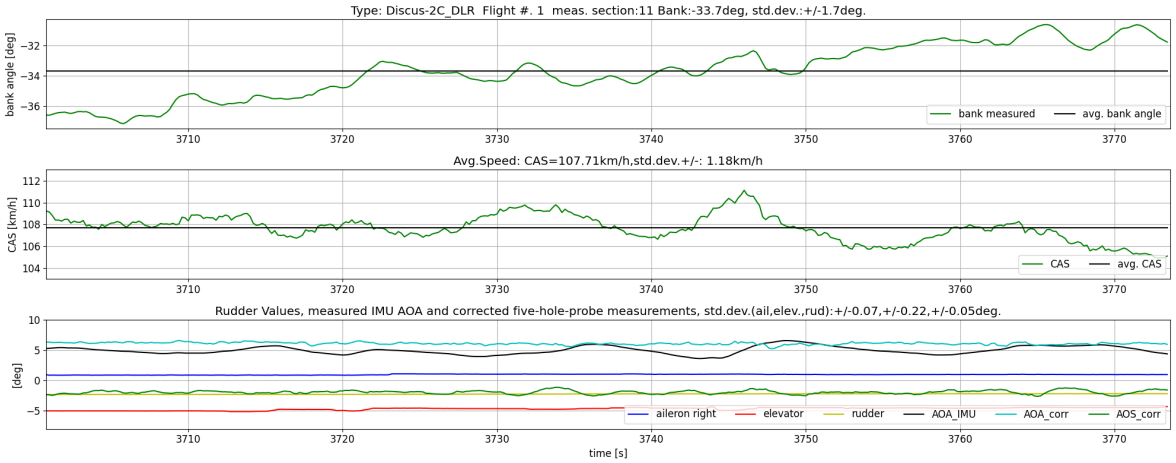

Figure 19: Section 1.11; overview of measured values

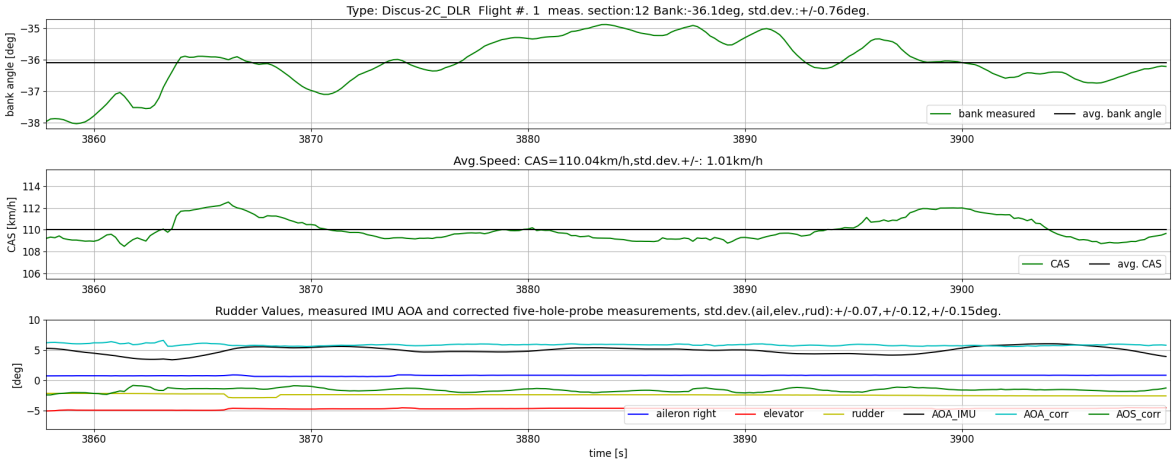

Figure 20: Section 1.12; overview of measured values

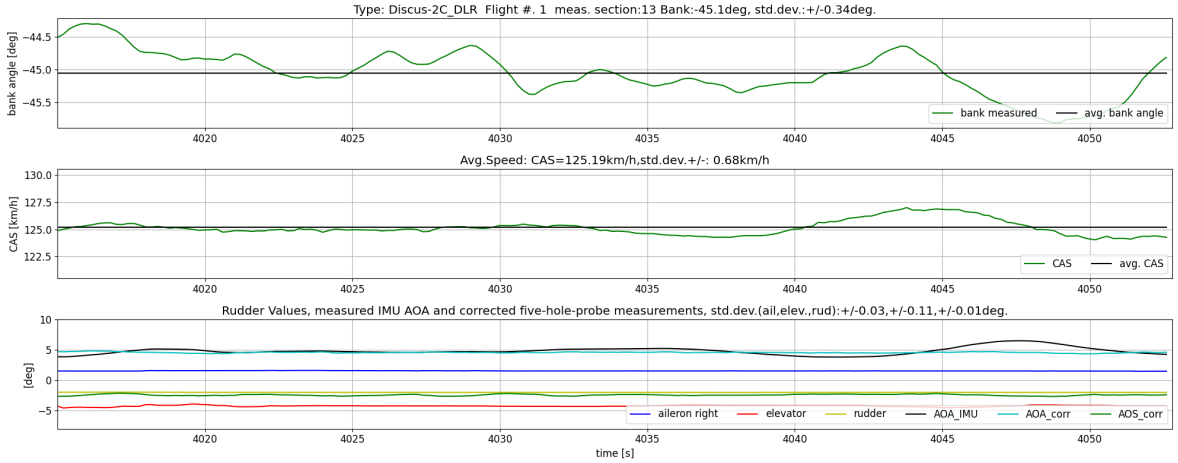

Figure 21: Section 1.13; overview of measured values

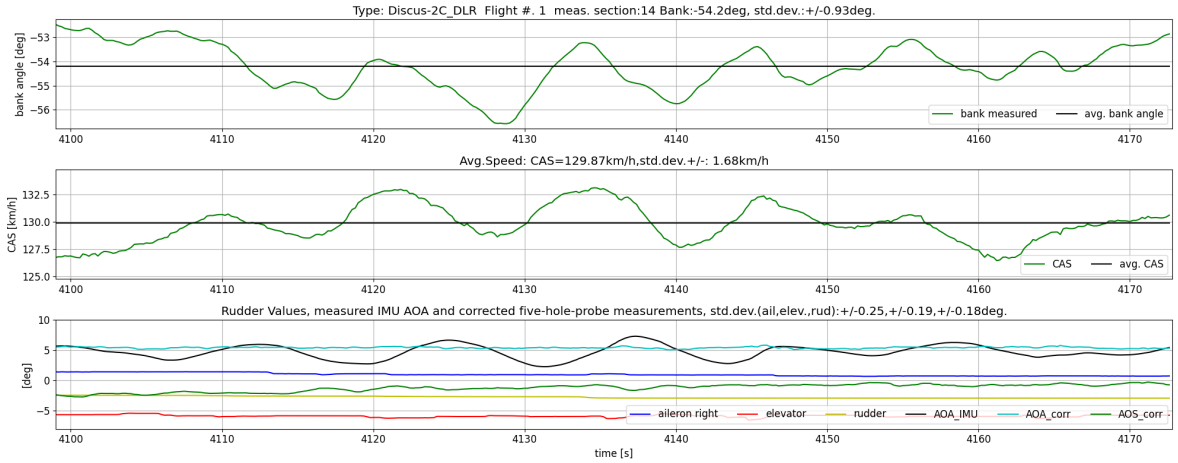

Figure 22: Section 1.14; overview of measured values

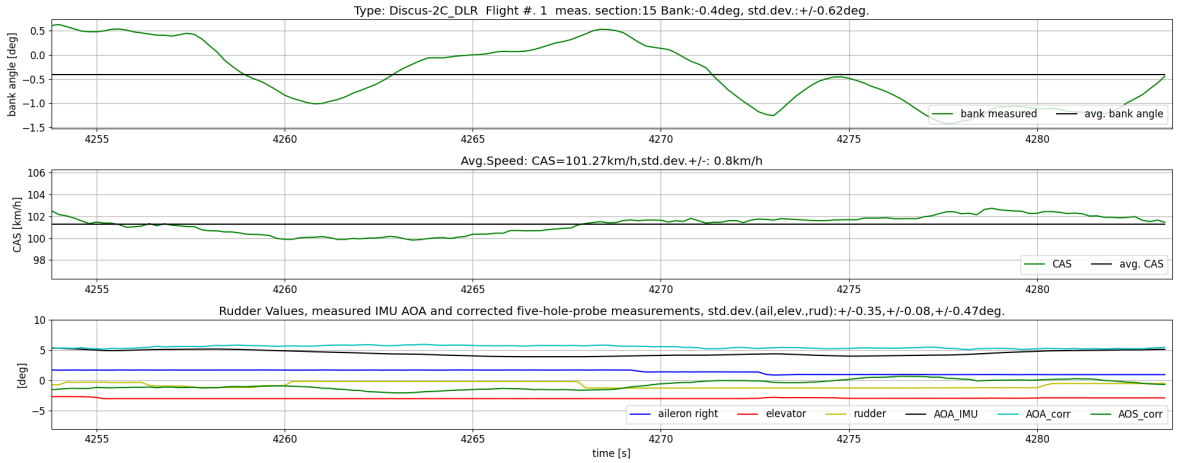

Figure 23: Section 1.15; overview of measured values

E. Measurement data plots of all measurment sections of Flight #2:

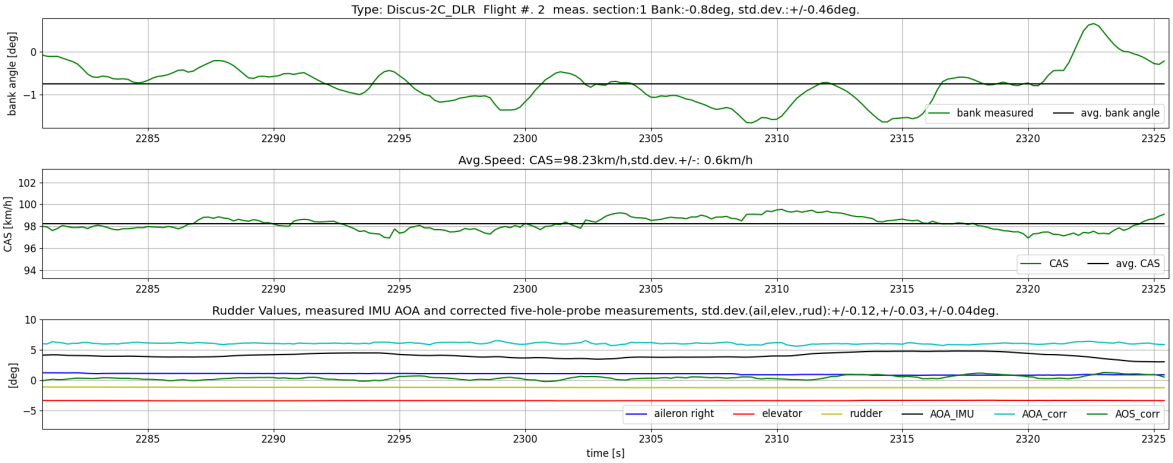

Figure 24: Section 2.1; overview of measured values

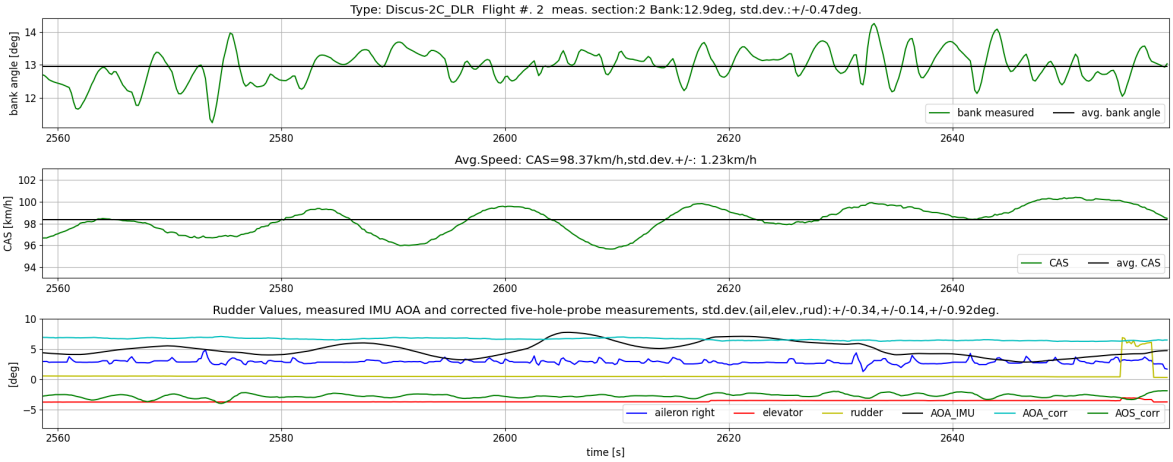

Figure 25: Section 2.2; overview of measured values

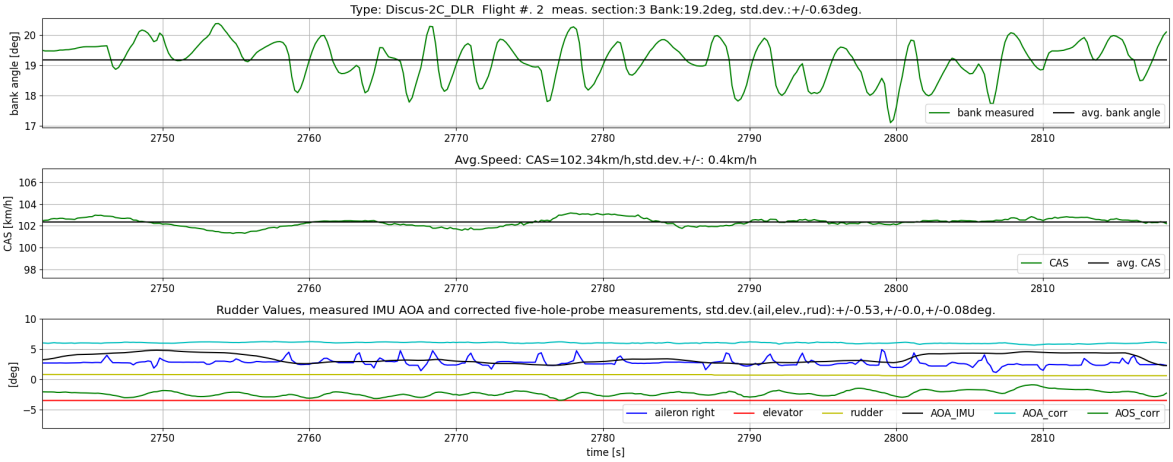

Figure 26: Section 2.3; overview of measured values

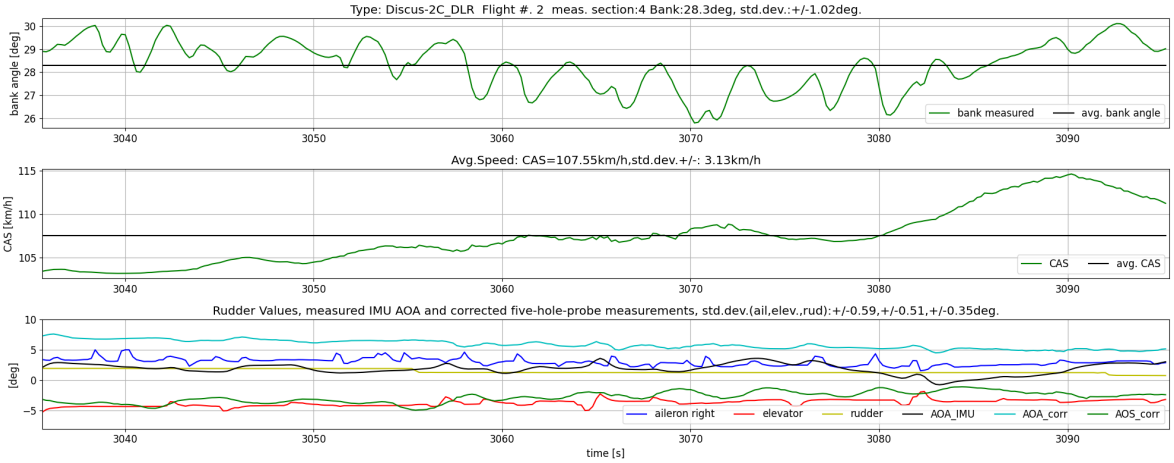

Figure 27: Section 2.4; overview of measured values

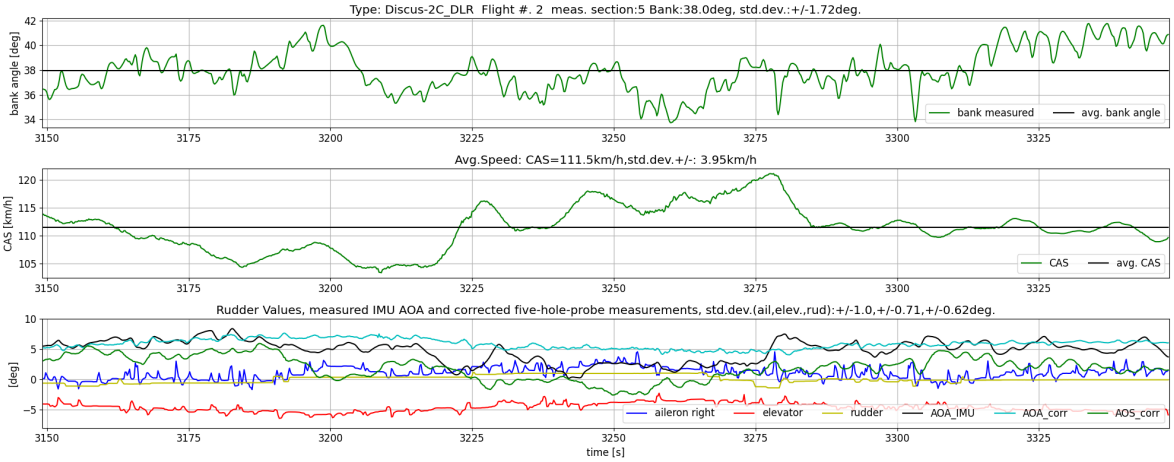

Figure 28: Section 2.5; overview of measured values

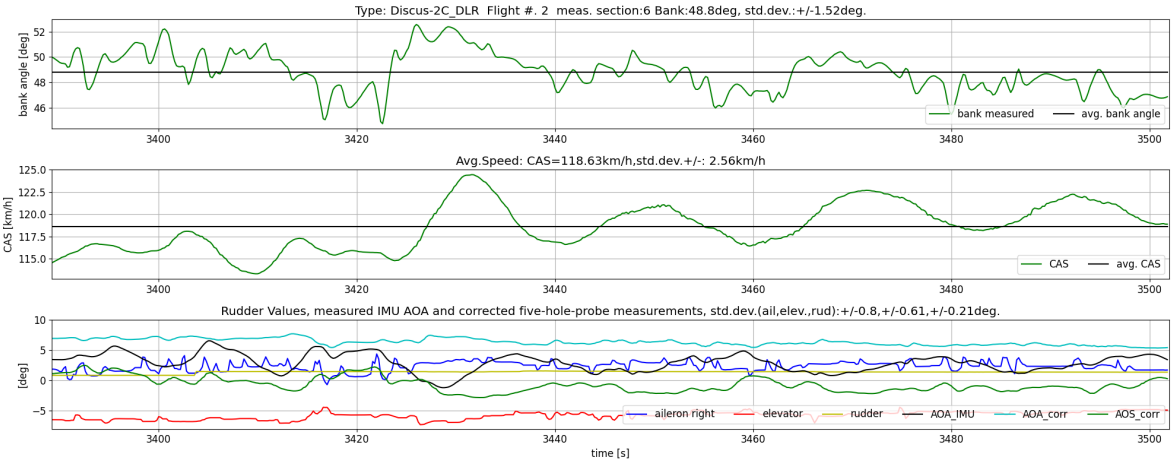

Figure 29: Section 2.6; overview of measured values

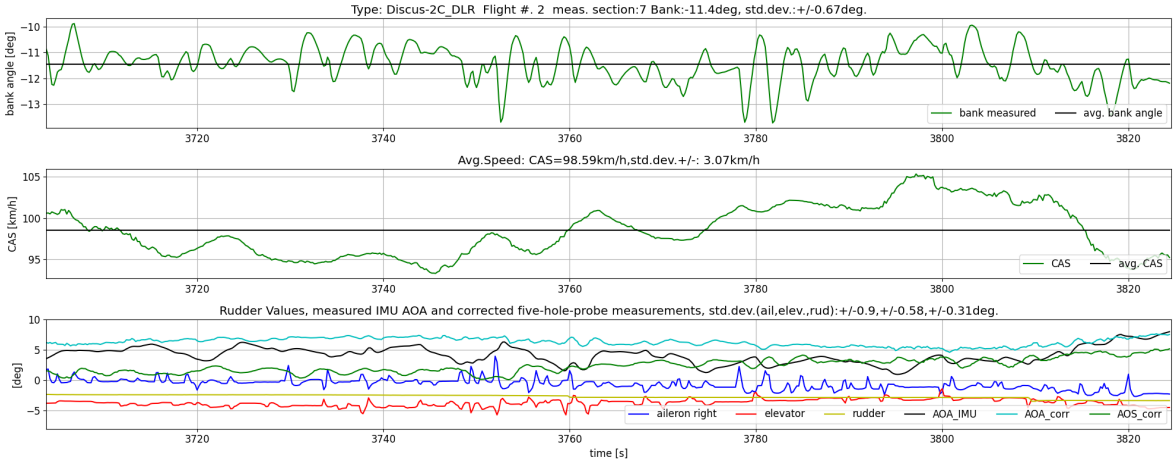

Figure 30: Section 2.7; overview of measured values

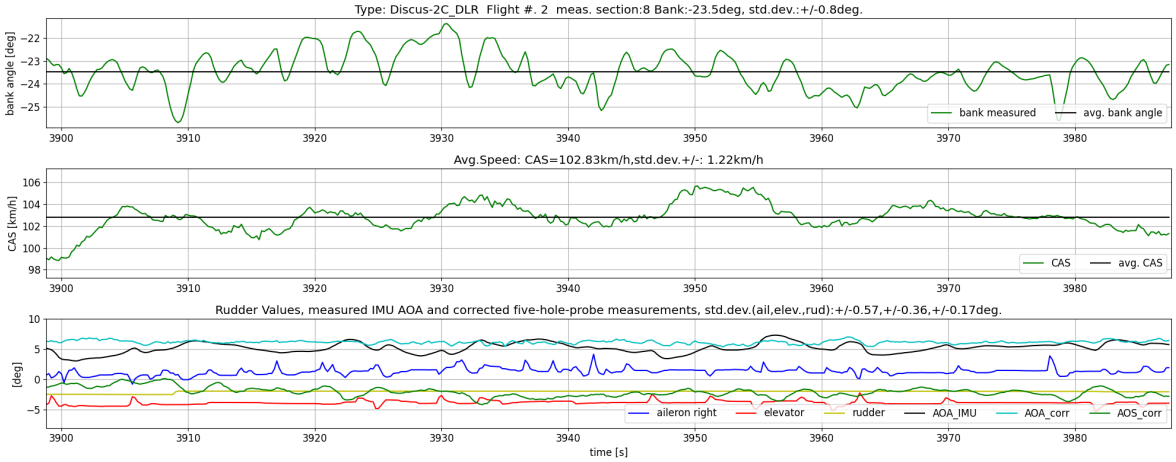

Figure 31: Section 2.8; overview of measured values

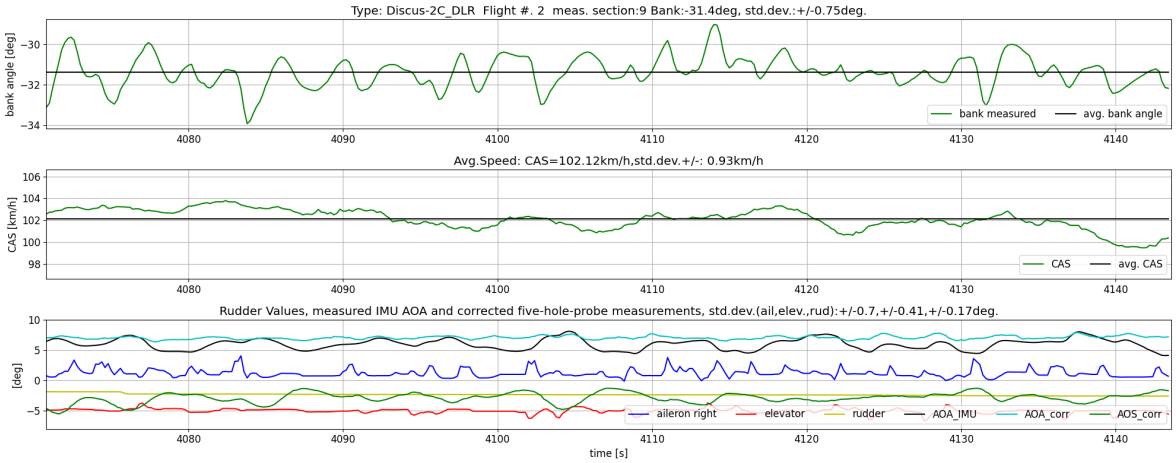

Figure 32: Section 2.9; overview of measured values

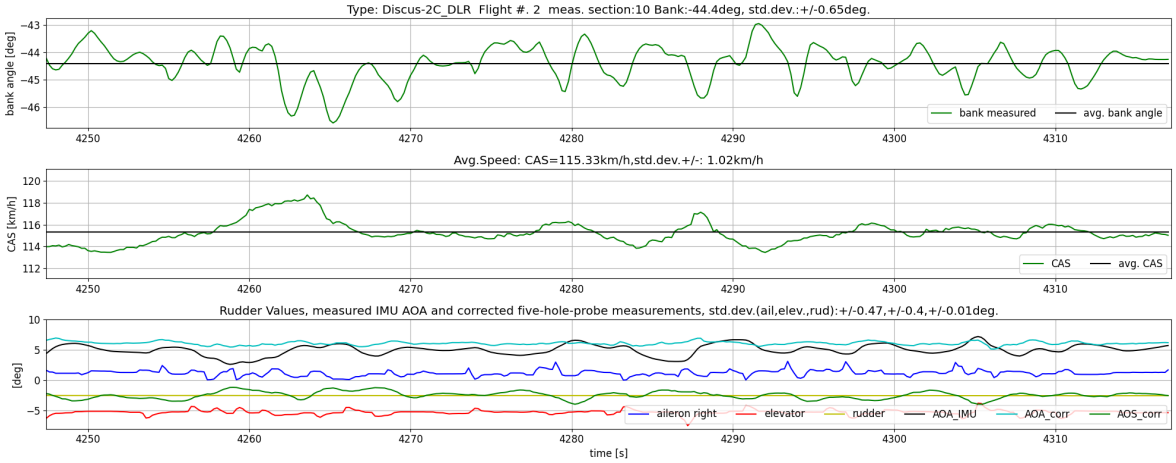

Figure 33: Section 2.10; overview of measured values

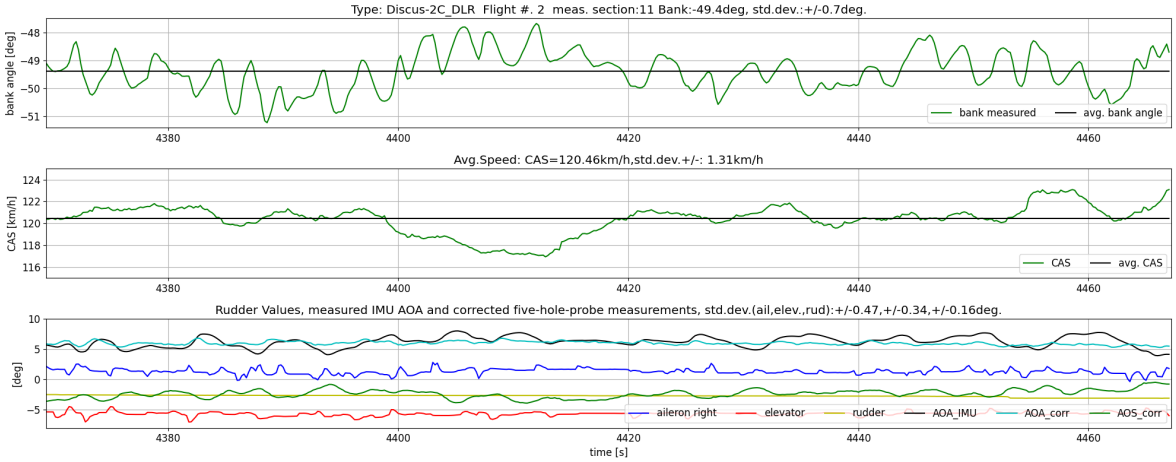

Figure 34: Section 2.11; overview of measured values

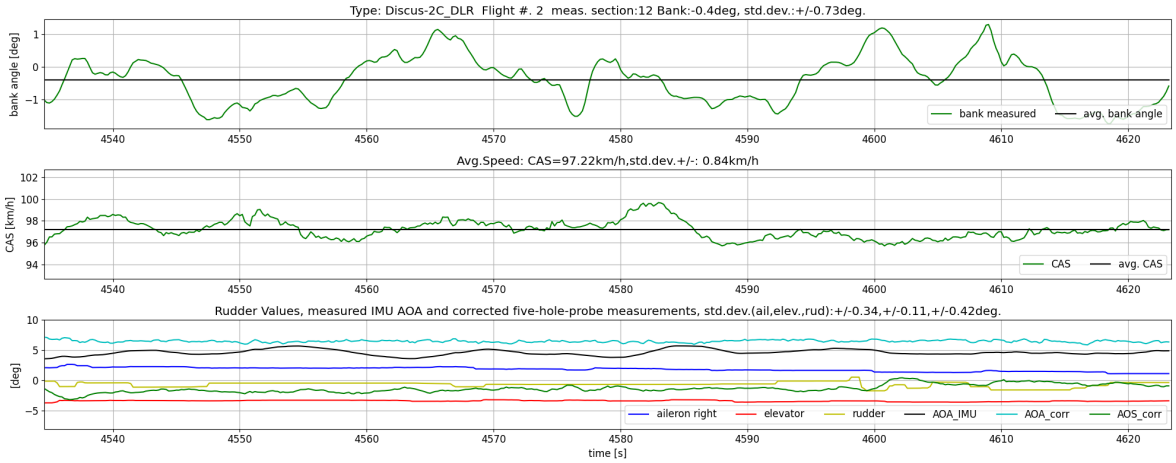

Figure 35: Section 2.12; overview of measured values